

Etalon interference wavelength metrology using webcams

J. Nicholas Porter

A senior thesis submitted to the faculty of
Brigham Young University
in partial fulfillment of the requirements for the degree of
Bachelor of Science

Dallin Durfee and Richard Sandberg, Advisors

Department of Physics and Astronomy
Brigham Young University

Copyright © 2020 J. Nicholas Porter

All Rights Reserved

ABSTRACT

Etalon interference wavelength metrology using webcams

J. Nicholas Porter

Department of Physics and Astronomy, BYU

Bachelor of Science

Many fields of research require precise wavelength measurement, but commercially available wavemeters are often too expensive, too large, or too fragile to be practical. We have designed and constructed a robust, compact, and inexpensive wavelength meter. The wavelength meter operates by analyzing the interference patterns caused by a series of etalons. Measuring this etaloning across a range of known wavelengths provides a set of wavelength-dependent reference functions that can be used to calculate an unknown wavelength within the same range. We present this device's design along with data measuring its accuracy and precision. Over a period of 24 hours from calibration, the device has an average error of 0.04 ppm with a standard deviation error of 3.94 ppm. Over a period of 400 hours from calibration, the average error rises to 0.90 ppm with a standard deviation of 5.29 ppm.

Keywords: metrology, optics, webcam, wavelength meter, wavemeter

ACKNOWLEDGMENTS

There are many people and organizations that have made the present work possible. I thank Brigham Young University for funding my research. I thank the engineers and designers at Adafruit, Bristol, Sony, Thorlabs, Newport, Agilent, and Toptica for creating the many devices and components that went into this work. I thank the developers of Python for designing and maintaining such a fantastic language. I thank my advisors, Dr. Durfee and Dr. Sandberg—the former for believing in me when *I* had no idea what I was doing, and the latter for believing in me when *he* had no idea what I was doing. I thank the other researchers in my lab, particularly Jarom Jackson and David Mckenna. Most of all I thank my incredible wife, Jenicca, who has probably sacrificed more for my research than I have. She is my angel.

Contents

Table of Contents	iv
List of Figures	vi
List of Tables	vi
1 Introduction	1
1.1 Wavelength metrology	1
1.2 Etalon interference	2
1.3 Prior work at BYU	4
1.4 Overview	5
2 Method	7
2.1 Device construction	7
2.1.1 Webcam	9
2.1.2 Etalons	9
2.1.3 Temperature control	11
2.2 Experimental setup	11
2.2.1 Multiple lasers	12
2.2.2 Setup phase	13
2.2.3 Data collection	14
2.3 Computation	15
2.3.1 Terminology	15
2.3.2 Calibration	15
2.3.3 Calculating wavelength	17
3 Results	19
3.1 Analysis	19
3.1.1 Overall precision	20
3.1.2 Measures of stability	22
3.1.3 Allan deviation	23
3.2 Discussion	25

3.2.1	High precision, low cost	25
3.2.2	Sources of error	25
3.3	Conclusion	26
3.3.1	Directions for further work	27
Appendix A Free spectral range and thick etalons		29
Appendix B Python code documentation		31
Appendix C Shutter system design		34
Appendix D Blue laser controller		35
Bibliography		37
Index		39

List of Figures

1.1	Schematic of the etalon effect	3
2.1	Basic schematic of the ELIAS wavelength meter	8
2.2	Potential beam paths through multiple etalons	11
2.3	Experimental setup	12
2.4	Flowchart of the experimental process	14
2.5	Pixel calibration	16
2.6	Minimized cost function for a single take	18
3.1	Error histogram	21
3.2	Error as a function of time	22
3.3	Error as a function of wavelength	23
3.4	Allan deviation error	24
C.1	Shutter control circuit	34
D.1	Laser control circuit	36

List of Tables

1.1	Comparison of various wavelength meters	2
2.1	Spectral ranges of lasers used	13
3.1	Conversions for wavelength and frequency	20
3.2	Comparison of ELIAS with other wavelength meters	25

Chapter 1

Introduction

1.1 Wavelength metrology

The ability to precisely measure a monochromatic light source's wavelength is necessary in many branches of research. Single-frequency lasers are used in atomic and molecular physics, usually because of light's ability to excite atomic and molecular transitions when tuned to just the right frequency. This phenomenon is useful in studying the transitions themselves but also has further applications. Cold atom research, for example, relies on the same principle to laser-cool individual atoms down to nearly absolute zero. In communications, wavelength division multiplexing (WDM) takes advantage of the wave nature of light by superimposing multiple transmitted signals at different wavelengths, then separating them on the receiving end. All of these techniques require some way of precisely measuring wavelength.

Many types of wavelength meters are commercially available, but the prices of these devices often pose a serious problem for their implementation. As Table 1.1 shows, the more precise the measurement, the more expensive the wavelength meter. Precision measurements also often require precision optics and moving parts, both of which are easily damaged. In addition to being expensive

Table 1.1 A table comparing various types of wavelength meters by precision, operational range, size, weight, and price. While technical specifications and prices vary, the examples given here are considered typical within their categories. Note that as the precision improves, the size, weight, and price all tend to increase.

Wavemeter Type	Precision	Dimensions, cm	Weight, kg	Price
Grating spectrometer [1]	<1.0 nm	5 x 11 x 15	0.57	\$6563
Integrating sphere [2]	0.2 nm	9 x 22 x 31	2.5	\$5514
Michelson interferometer [3]	0.1 pm	15 x 32 x 48	12	\$28 026

and fragile, precision wavelength meters are often large, heavy, and use a lot of power. Such drawbacks hinder many laboratories and research groups who might otherwise make significant contributions to the aforementioned fields and others.

Many alternative wavelength meter designs have been proposed in an attempt to address some of the drawbacks to currently available wavelength meters. Nabiev *et al.* [4] used a pair of photodiodes with a wavelength-dependent reflector between them. Photons not detected by the first diode have a certain probability of being transmitted to the second, and the wavelength can be calculated by comparing the two diodes' measurements. Mazilu *et al.* [5] used a stationary random diffuser to scatter laser light in a wavelength-dependent speckle pattern. Gray *et al.* [6] used a modified Fizeau interferometer to produce wavelength-dependent interference fringes. While these and other advances have been made, low-cost wavelength metrology continues to need improvement.

1.2 Etalon interference

Our proposed solution to this challenge uses wavelength-dependent interference fringes produced by a series of etalons. An etalon is a pair of flat, parallel surfaces, placed perpendicular to a beam, such that the index of refraction between the surfaces is different than on either side. When a beam

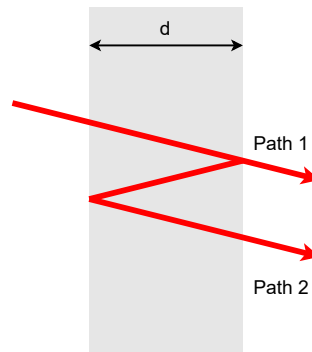


Figure 1.1 Schematic of the etalon effect. Two potential paths for a beam of light travel through an etalon of thickness d . Path 2 covers an extra distance of $2d$ compared to path 1. The relative phase shifts of the two paths determines how they will interfere with each other upon exiting the medium. In reality, the two paths overlap and are perpendicular to the film; they have been separated for illustration.

of light passes through an etalon, part of it is reflected internally. When the internal reflection is finally transmitted, it has picked up a phase shift from its longer path. The overall transmitted beam, therefore, is a superposition of beams with different phases, as shown in Fig. 1.1. If the extra distance covered by the reflection path equals an integer number of wavelengths, then the two exiting beams constructively interfere; if it is an integer plus a half number of wavelengths, then the beams destructively interfere. The final transmission is represented by the function $T(\lambda, d)$, which varies between peaks and troughs based on the number of wavelengths that "fit" inside the etalon. This phenomenon is called etalon interference or etaloning. The change in wavelength needed to go from one peak to the next is called the free spectral range (FSR) of the etalon.

Etaloning is commonly seen and utilized in thin films, where the thickness d is on the order of a wavelength. Thick-film etaloning is rarely observed in day-to-day life because it is much more sensitive to small changes in thickness and wavelength (see Appendix A). When broadband light passes through an ordinary thick film (*e.g.* sunlight through a window), this sensitivity prevents the observation of etaloning. First, nanometer-scale variations in thickness cause peaks and troughs to occur right next to each other and wash each other out. Second, wavelengths that interfere

constructively and those that interfere destructively are too close to be distinguished.

With the right parameters, however, this sensitivity makes etalon interference ideal for detecting small differences in wavelength. In fact, Konishi *et. al.* [7] developed a system of four Fabry-Perot etalons that was able to measure wavelength as accurately as 0.1 ppm. However, the price of Fabry-Perot optics [8] still prevents this design from being a low-cost, high-precision wavelength meter.

1.3 Prior work at BYU

In 2015, our research group at BYU began designing an inexpensive wavelength meter based on a commercially available color sensor chip [9–11]. These chips are commonly found in computer monitors and television screens and are used to gauge the general color of the ambient light in the room so that the display can adjust accordingly. Each chip has an array of red, green, blue, and white (RGBA) filtered photodiodes. By comparing the relative values measured by each color to the known spectral response functions, we were able to calculate wavelength.

We found that the color filters in front of the photodiodes were acting as etalons for the monochromatic light. Because the chips were designed for broadband light, the spectral response functions did not take etaloning into account. As a result, the wavelength calculations showed a systematic error [9]. However, if the calibration were to include the etaloning effects, the resulting function would contain fine features that could be used for a more precise calculation.

By including the etaloning effects in the calculations, we were able to achieve an accuracy of 11.5 ppm and a precision of 8.46 ppm over a 41.5-hour period [10, 11]. However, we decided that the color sensor was not ideal for this type of calibration for two main reasons: its pixels are too large, and it lumps together the measurements of same-color pixels. Both of these factors wash out the etaloning and limit its usefulness. A better detector was needed.

As imaging technology advances, the image sensors in small cameras get smaller, denser, and cheaper to manufacture. Many optics laboratories have begun taking advantage of this by using webcams as an inexpensive alternative to purpose-built optical detectors [12, 13]. The pixels on a typical webcam image detector are orders of magnitude smaller than those of the color sensor, and measured individually, making a webcam an ideal replacement for this experiment. Therefore, we decided to develop a new device, based on similar principles, but using a webcam in place of the color sensor.

1.4 Overview

The device that we have developed uses a webcam to measure thick-film etaloning over a range of known wavelengths. These initial measurements form a calibration, which can then be used to calculate an unknown wavelength within the same range. I call this method Etaloning Laser Interference Analysis Spectrometry (ELIAS).

The ELIAS method is not without drawbacks. As covered in this thesis, imperfect temperature control leads to picometer-scale drift in the calibration and is the main cause of wavelength calculation error. Additionally, periodicity in the webcam's spectral response can lead to aliasing if calibrated on too wide a range. These problems are caused by flaws in the implementation rather than the principle and can, therefore, be addressed without fundamentally changing the design. More importantly, the trade offs in these areas come with some impressive benefits.

The primary benefit that ELIAS offers is low-cost precision. It measured wavelengths with standard deviation errors as low as 2.9 ppm over a 24-hour period and 5.02 ppm over a sixteen-day period. Yet by not requiring precision optics—the most expensive part of most wavelength meters—it can be built with less than \$100 worth of hardware. In addition to being inexpensive, the method is robust, compact, easy to build, and doesn't require high-voltage electrical power.

In this thesis, I will describe the design and testing of an ELIAS wavelength meter, and explain the results of our testing in detail. Chapter 1 has discussed the motivation and theory behind the experiment. Chapter 2 deals with experimental methods, with sections describing the device's construction, the experimental setup used to test it, and the computational methods it uses to calculate wavelength. Chapter 3 discusses the results of the experiment, what those results mean, and what directions this research can be taken in the future. Appendix A discusses the concept of free spectral range and shows why thick-film etaloning is more sensitive to wavelength and thickness than thin-film etaloning. Appendix B explains some of the key features of the Python package I developed to run and analyze this experiment [14]. I have also written an article on the ELIAS project, which has been published in Optics Express [15].

Chapter 2

Method

In this chapter, I describe the design and operation of the ELIAS device, the experimental setup used to test it, and the computational methods it uses to determine wavelength. The fully annotated Python code I developed for the experiment and analysis can be found online [14].

2.1 Device construction

A schematic of the ELIAS device is shown in Fig. 2.1. It consists of a webcam, several etalons, an aluminum box with a fiber-optic input, and various electronics, including a Raspberry Pi (RPI) single-board computer and a temperature controller. Monochromatic light from a single-mode fiber passes through the etalons before being detected by the webcam. The etalon interference patterns thus measured are used to calculate the light's wavelength. A temperature controller prevents thermal expansion and ensures that the etaloning depends only on wavelength. The single-mode fiber ensures that only a single wavelength is measured at a time. The primary components of the ELIAS device are now described.

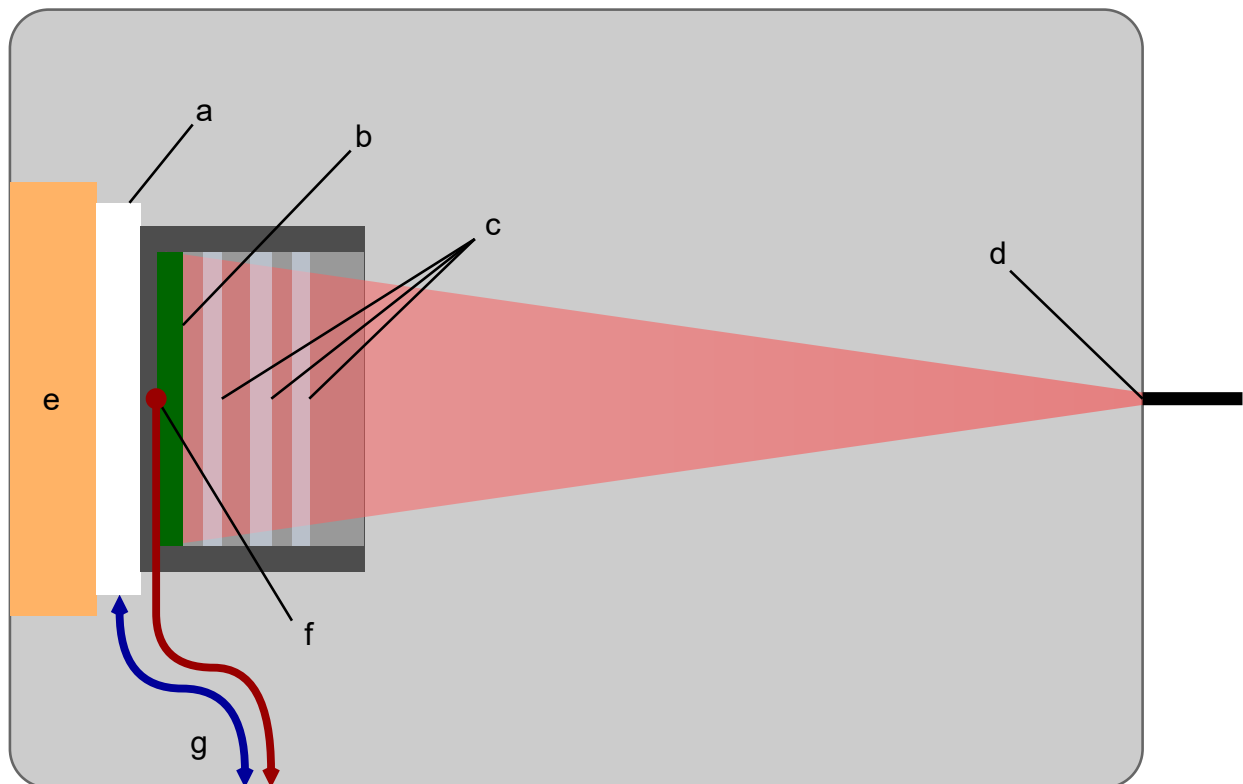


Figure 2.1 Basic schematic of the ELIAS wavelength meter, *not to scale*. Marked on the diagram are: (a) a thermoelectric cooler (TEC), (b) a webcam photodetector, (c) three microscope slides acting as etalons, (d) a single-mode optical fiber, (e) a copper heat sink, (f) a thermistor, and (g) wires connecting the thermistor and TEC to an external temperature controller. The gray box represents an aluminum enclosure.

2.1.1 Webcam

We used a Raspberry Pi Camera Module V2 [16] which contains a Sony IMX219 image sensor [17]. We chose this particular webcam for several reasons. First, it interfaces natively with the RPi, which was conveniently sized and priced for our purposes. Second, although its pixels only capture 10-bit data (compared to the 16-bit data collected by the color sensor [9–11]), its photoarray has 8.08 million pixels, whereas the color sensor effectively has four. Having more pixels means more independent measurements of the light and leads to improved accuracy.

The final and most important reason for choosing the Pi Camera is that its Python package provides easy access to raw images on the individual-pixel level. By contrast, the color sensor summed the response from all pixels of the same color into a single measurement. If one pixel saw a bright fringe where another saw a dark fringe, this summing process would effectively wash them both out, reducing the interference's usefulness. Measuring each pixel independently prevents this washing-out effect.

2.1.2 Etalons

In Appendix A, I show that etalon interference becomes extremely sensitive as the etalon's thickness becomes much greater than the light's wavelength. Because of this sensitivity, Fabry-Perot etalons are made "optically flat"—sometimes deviating no more than a few nanometers in thickness across the entire optic. While this level of flatness ensures a very uniform interference pattern, it is expensive to manufacture. ELIAS is chiefly meant as a low-cost alternative, so precision optics are not ideal.

Instead, we used microscope slides and slide cover slips on the key assumption that their reflective surfaces could be considered optically flat across a small enough area, even if they're not optically flat across the whole surface. The ELIAS etalons (Fig. 2.1c) only need to be flat over the cross-sectional area of a path travelling from the end of the optical fiber to a single pixel. The end of

a single-mode fiber is a few micrometers in diameter, and the pixels on the IMX219 are $1.12\ \mu\text{m}$ on a side [17]. This allows for a kind of "imperfect flatness" on scales larger than a few micrometers.

In fact, the imperfect flatness is an advantage. Each pixel receives the light travelling through a unique part of the slide and therefore measures a unique interference pattern. Ideally, this allows each pixel to have a linearly independent spectral response function. However, the thickness of a microscope slide doesn't vary enough to significantly affect the FSR (Appendix A shows mathematically why this is the case). Having the same FSR across all pixels causes two interrelated problems.

First, it limits the region of wavelengths that ELIAS can measure to the FSR of the etalon. Adjacent interference fringes are effectively identical, therefore a calibration that extends across multiple fringes cannot distinguish between them. This leads to aliased measurements. The second problem is that, even within an appropriate wavelength region, each pixel's spectral response represents an interval of a periodic function. Any part of a pixel's response function that overlaps with any part of any other pixel's response is no longer linearly independent, largely undermining the advantage of imperfect flatness.

Fortunately, both problems are fixed by replacing the single etalon with a system of multiple etalons. When light passes through multiple etalons, each interface creates new potential paths for the beam to travel. The overall transmission is the product of the etaloning between each pair of surfaces:

$$T(\lambda, d) = \prod_m T_m(\lambda, d). \quad (2.1)$$

Figure 2.2 illustrates some of the paths that could be taken through a system of three etalons. The interference pattern that results from such a system has a larger FSR than any of the individual etalons. Through trial and error, I found that a stack of three etalons—a 0.5 mm microscope slide and two 0.1 mm cover slips—the pixel responses can be considered independent enough to perform wavelength calculations over the tuning ranges of our lasers without aliasing.

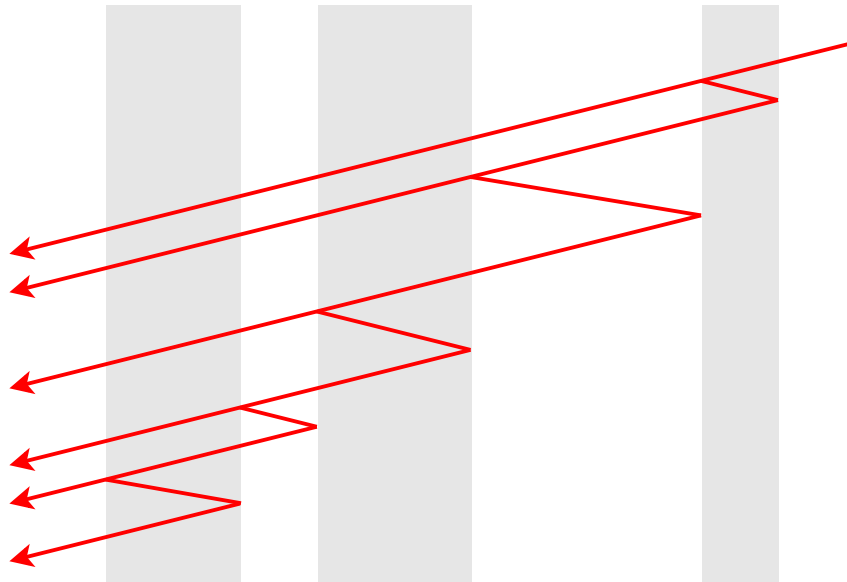


Figure 2.2 Potential beam paths through multiple etalons. As in Fig. 1.1, the various paths have been separated for illustration.

2.1.3 Temperature control

Because etalon interference is highly sensitive to small changes in thickness, thermal expansion of the etalons could easily ruin the calibration. To prevent this, the camera and etalons are temperature controlled using a thermo-electric cooler (TEC) and a thermistor (Fig. 2.1a, f). An ILX Lightwave LDT-5412 temperature controller [18] constantly measures and adjusts the TEC's output to maintain a constant temperature. While the controller itself costs a few hundred dollars, a simple feedback controller can be programmed into the RPi. Therefore, I do not count the temperature controller in the cost of the device.

2.2 Experimental setup

The experiment is configured as shown in Fig. 2.3, so that a monochromatic beam can be simultaneously measured by both the ELIAS device (j) and a Bristol 521 Michelson-interferometer

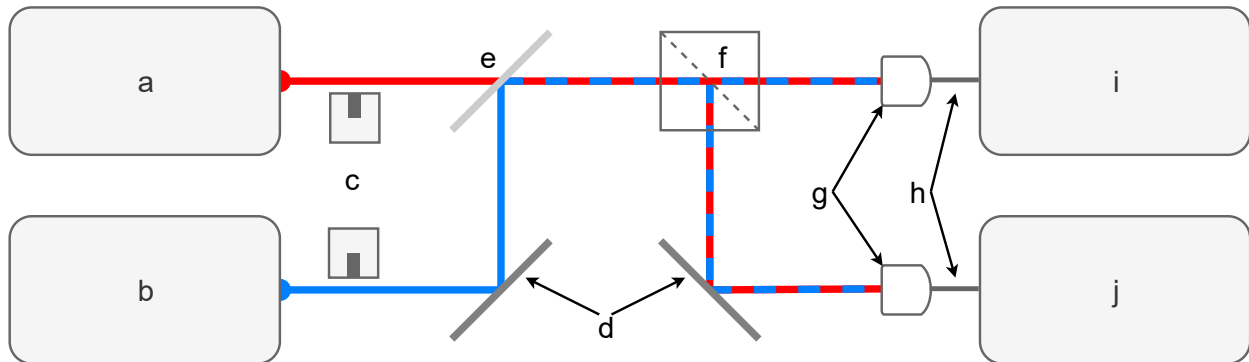


Figure 2.3 A simplified diagram of the experiment. Marked on the diagram are (a) a 657 nm (red) tunable-diode laser, (b) a 460 nm (blue) tunable-diode laser, (c) remote-controlled shutters, (d) mirrors, (e) a dichroic beam splitter, (f) a cubic beam splitter, (g) fiber couplers, (h) single-mode optical fibers, (i) a Bristol 521 wavelength meter, and (j) the ELIAS wavelength meter. Although, in practice, the two laser shutters are only opened one at a time, the diagram shows both open.

wavelength meter (i). The additional wavelength meter allows us to calibrate the ELIAS device and provides a standard for later measurements to be compared against. The experiment is controlled from the RPi, but due to compatibility issues, an additional computer is needed to interface with the Bristol 521.

2.2.1 Multiple lasers

In order to understand the ELIAS device's performance over different regions of the visible spectrum, we measured two tunable-diode lasers (TDLs) in this experiment (Fig. 2.3a, b). TDLs are ideal for testing a wavelength meter because they provide a stable, monochromatic beam that can be adjusted or "tuned" over a small range of wavelengths. The tuning ranges for each are given in Table 2.1. The red laser is controlled digitally via USB; the blue is controlled with an analog voltage produced by rectifying a pulse-width-modulation (PWM) signal from the RPi's general purpose input/output (GPIO) terminals. The

I designed and constructed an automated shutter system (Fig. 2.3c) to block one laser while the

Table 2.1 The minimum and maximum wavelengths (λ_{\min} , λ_{\max}) as well as the absolute tuning range ($\Delta\lambda$) for each of the two lasers used in this experiment.

Color	λ_{\min}	λ_{\max}	$\Delta\lambda$
Red	657.358 nm	657.539 nm	181.5 pm
Blue	460.765 nm	460.875 nm	109.4 pm

other is being measured. The shutters allow the experiment to take data alternately from both lasers without requiring either to be powered down or realigned. The design of these shutters is described in Appendix C.

Even though only one shutter is open at a time, the two beam paths must be identical in order to couple into the two fibers (Fig. 2.3h). Beams of different wavelengths can be joined onto one path with minimal power loss by a dichroic beamsplitter, which reflects some wavelengths and transmits others. The dichroic in our experiment (Fig. 2.3e) transmits red light and reflects blue. A cubic beamsplitter (Fig. 2.3f) is then used to couple either beam into both wavelength meters.

2.2.2 Setup phase

The Python software which I developed to control the experiment executes the process shown in Fig. 2.4. Before beginning data collection, the program performs a setup phase (depicted in violet). During the setup phase, the program initializes the ELIAS device for taking data and runs diagnostics to ensure that each part of the experiment is working properly.

In order to reduce computational time, only 1000 pixels on the webcam are used for measurement. The coordinates of these pixels are selected based on a Monte Carlo distribution and saved to ensure that the same pixels are measured every time data is collected. Additionally, camera parameters (*e.g.* exposure time, gain, white balance, etc.) are fixed to prevent them from re-adjusting for each measurement. Finally, the program tests the shutters, lasers, and Bristol wavelength meter. If there

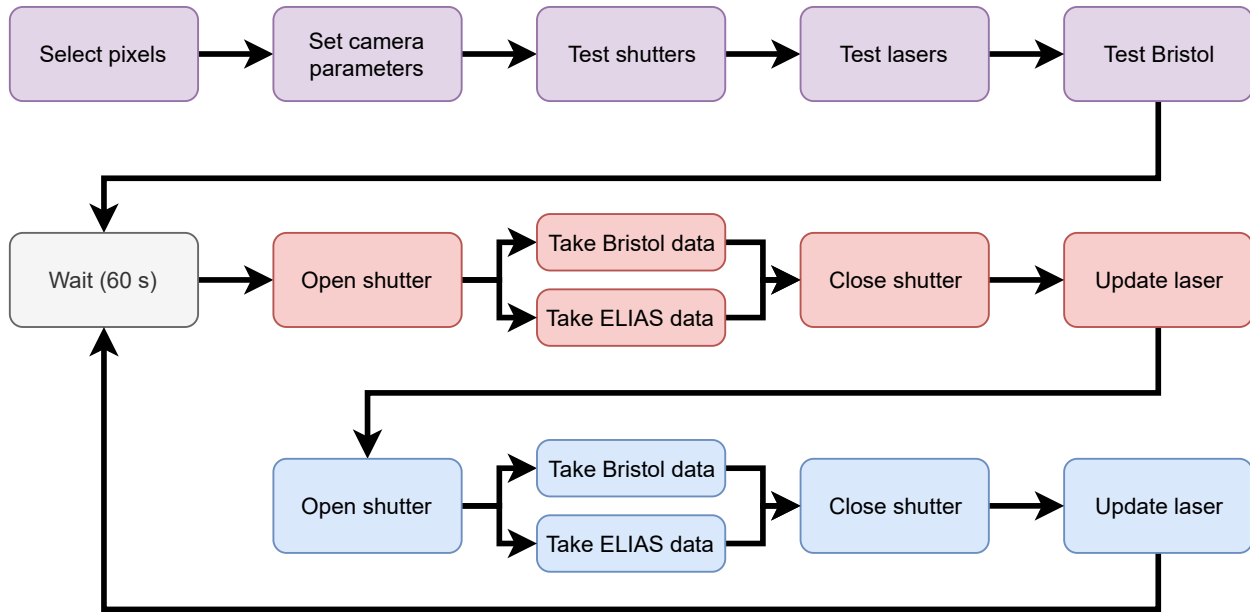


Figure 2.4 Flowchart of the experimental process. The setup phase is depicted in violet; the red and blue steps correspond to the red and blue lasers.

are any issues (*e.g.* a shutter won't open, a laser doesn't respond), the program aborts the experiment so it doesn't waste time collecting bad data. This assurance is especially useful when running the experiment remotely through a web server.

2.2.3 Data collection

The data collection phase is shown in Fig. 2.4 as the gray, red, and blue processes. The RPi opens one laser's shutter, reads the measurement from both the Bristol wavemeter and the ELIAS device. The ELIAS device measures by taking five successive pictures with the webcam and then summing and recording the values of each pixel selected in the the setup phase. The RPi then closes that shutter, and tunes that laser's wavelength to a new, random value. Updating the lasers' wavelengths at the end of each take gives them time to settle before being measured again.

This process is then repeated for the other laser. After both lasers have been measured, the device waits for 60 seconds. During this downtime, the camera constantly takes and discards pictures (as if

it were still taking data), which prevents the camera from cooling between takes. The collection phase then repeats.

The data presented in this thesis were taken over a period of 400 hours (just under 17 days). In order to develop the analysis process, I programmed the experiment to only collect raw data rather than calculating the wavelength with each take. The actual calculations are done after a whole set of measurements has been taken.

2.3 Computation

2.3.1 Terminology

Before proceeding, several terms should be defined to avoid ambiguity. A "take" is a single experimental measurement of a laser set to a certain wavelength—one execution of the data collection phase. The "actual wavelength" (or λ_0) of a take refers to the wavelength measured by the Bristol 521. The "guessed wavelength" (or λ') is a temporary parameter used in calculation. The "calculated wavelength" (or λ_{calc}) of a take refers to the wavelength calculated by the ELIAS device.

2.3.2 Calibration

The ELIAS device calculates wavelength by comparing each pixel's measurement to a calibration function. Calibrating involves first tuning the laser to 100 random wavelengths and recording both the wavelength (as measured by the Bristol 521) and the response of each pixel on the webcam (normalized to account for changes in brightness). We can then define the calibrations for each pixel by fitting a polynomial to the resulting data. Figure 2.5 shows an example of the calibration data and functions for four arbitrarily chosen pixels.

Because of the variety in the pixels' responses, I developed an iterative method which allows

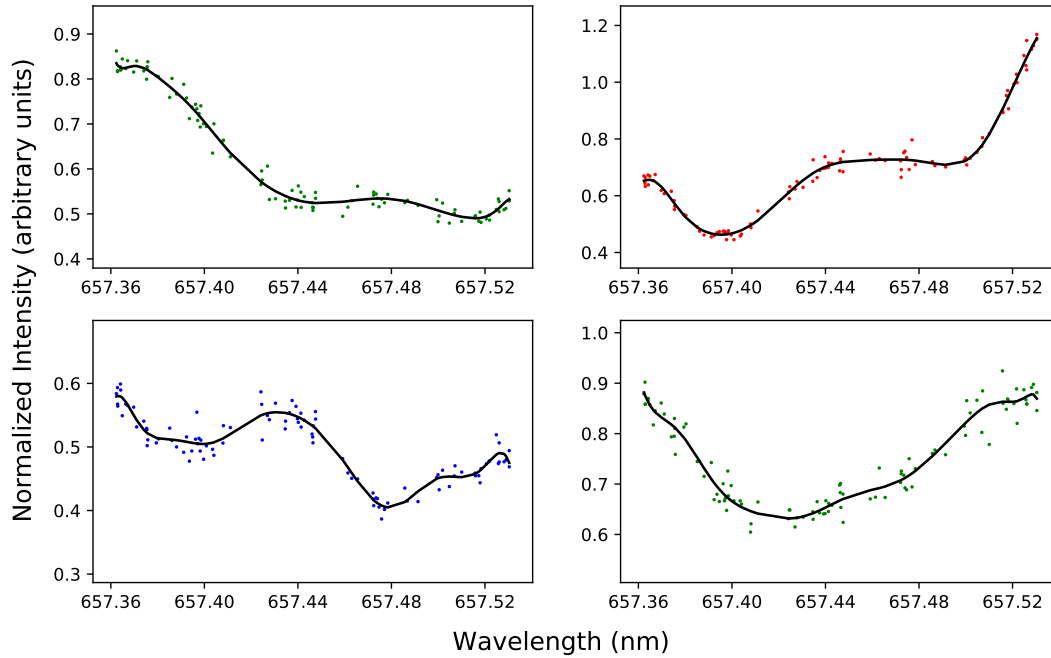


Figure 2.5 Calibration data & functions for four selected pixels. Each pixel’s response is measured at 100 different known wavelengths, and a polynomial function is fit to the resulting data. Unknown wavelengths can be calculated by measuring those pixel’s responses and comparing them to their respective calibration functions. The data points in these charts are colored to match their RGB pixel colors.

the calibrations to match the fine features on some pixels without fitting to noise on others. It begins with a linear (first-order polynomial) fit, and records the fit residual ϵ . The fit quality Q is then defined as,

$$Q_n = \frac{N\bar{y}}{\sqrt{\epsilon_n}}, \quad (2.2)$$

where n is the polynomial order, N is the number of takes used for the calibration, and \bar{y} is the average intensity of the calibration data. The fit order is incremented until any of the following

conditions are met:

$$Q_n > 250, \quad (2.3)$$

$$\frac{Q_n}{Q_{n-1}} < 1.01, \quad (2.4)$$

$$n = 15. \quad (2.5)$$

2.3.3 Calculating wavelength

We use a least-square-error method to calculate the wavelength by minimizing a cost function of a guessed wavelength λ' . For a given take, $C(\lambda')$ is defined as

$$C(\lambda') = \sum_p (f_p(\lambda') - y_p)^2, \quad (2.6)$$

where p is an arbitrary index given to each pixel, $f_p(\lambda')$ is the p -th pixel's calibration function, and y_p is the p -th pixel's measurement. In other words, $C(\lambda')$ is the sum over all pixels of the squared difference between a pixel's measurement and the value of its calibration function at the guessed wavelength λ' .

The contribution of a given pixel p is smallest at points where $f_p(\lambda') \approx y_p$, which may occur at multiple wavelengths. Most of these minima will be washed out by the non-minimal contributions of other pixels. However, near the actual wavelength, every pixel should measure close to its calibration function. The absolute minimum of $C(\lambda')$ should occur where $\lambda' \approx \lambda_0$. In fact, if the calibration were perfect (*i.e.* $f_p(\lambda_0) = y_p$ for all pixels at all wavelengths), then $C(\lambda_0)$ would be zero.

The value of λ' that minimizes $C(\lambda')$ is designated as λ_{calc} . An example of this is shown in Fig. 2.6. I wrote a Python program to numerically find λ_{calc} for each take. On my laptop (Intel Core i7-8550U processor, 16GB RAM), this analysis can be done in about 8 ms per take.

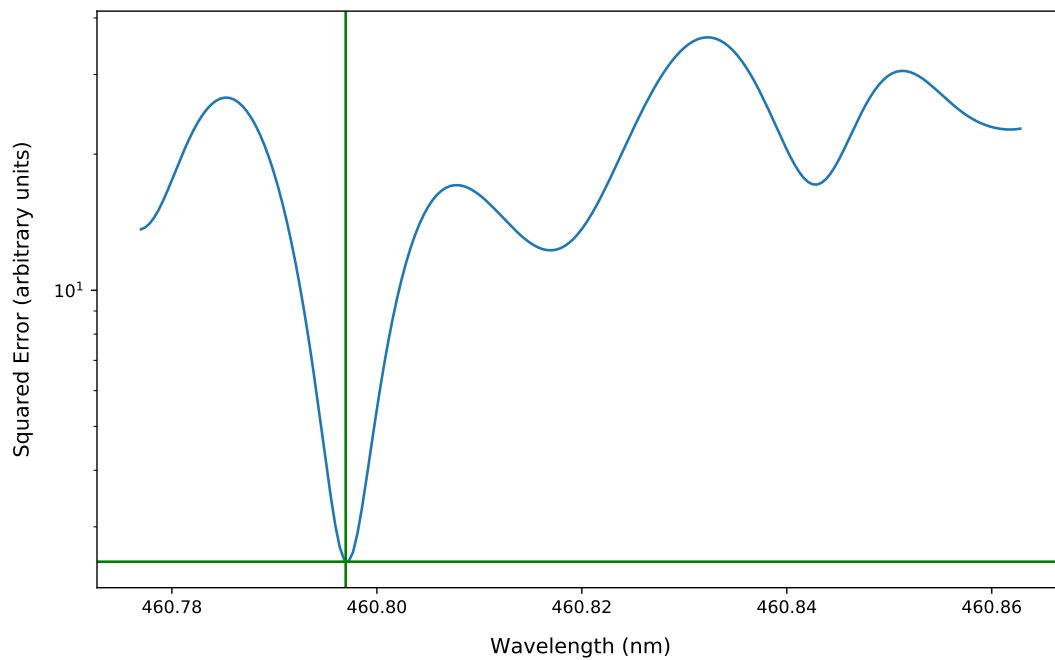


Figure 2.6 An example of the minimized cost function $C(\lambda')$ for a single take. The horizontal line shows the minimum value of $C(\lambda')$, and the vertical line shows the calculated wavelength, λ_{calc} .

Chapter 3

Results

In this chapter, I examine the precision and accuracy of the ELIAS device and discuss factors that may affect these measures. I also discuss potential directions for further work. I conclude that the ELIAS method of wavelength metrology is an excellent low-cost alternative to commercially available wavelength meters.

3.1 Analysis

The precision of any wavelength meter is typically taken as a standard deviation error in either wavelength or frequency over repeated measurements. These, in turn, can be given in various units. While each form has its uses, I have chosen to use wavelength-parts per million in this thesis, because it scales linearly with wavelength. This makes it easier to compare measurements made on the two lasers. It is also quite intuitive—one part per million is a single sheet in a stack of paper 100 meters high, or a single hair on ten peoples' heads. Table 3.1 provides factors that convert wavelength-parts per million into picometers or gigahertz (wavelength or frequency, respectively) for each of the two lasers.

Table 3.1 Conversion factors to convert wavelength-parts per million into picometers or into gigahertz for each of the two lasers.

Wavelength	Frequency	1 ppm→pm	1 ppm→GHz
657.45 nm	455.99 GHz	0.657	0.456
460.85 nm	650.52 GHz	0.461	0.651

3.1.1 Overall precision

As explained in Section 2.2.3, the present data was taken from both lasers each minute for 400 hours, resulting in over 36 000 total wavelength measurements. We compared the wavelengths calculated by the ELIAS device to those measured by the Bristol wavelength meter. For the red laser, ELIAS calculated wavelength with a mean error of 4.82 ppm and a standard deviation error of 5.16 ppm. For the blue laser, the mean was 1.63 ppm and the standard deviation was 8.12 ppm.

These errors were larger than anticipated, possibly due to transient temperature fluctuations in the earliest part of the data—the part used for calibration—as the temperature controller stabilized. If the first 200 measurements (about three hours of data) are excluded, the mean error reduces to 0.09 ppm for the red, 1.71 ppm for the blue, and the standard deviation error reduces to 5.12 ppm for the red, 5.45 ppm for the blue. This puts the overall precision of the ELIAS device just over ± 5 ppm over a period of 400 hours.

Because the early transients are likely caused by inadequate temperature control, they represent a flaw in the implementation, rather than the design. Thermal stability can be improved without any significant change in the way the device works. The truncated data is therefore a better representation of the ELIAS method than the full set.

The distribution of errors is shown in Fig. 3.1. The apparent bimodal distribution in the red laser data is related to time-based drift (see Section 3.1.2 and Fig. 3.2). Apart from that, the error for both data sets approximates a normal (Gaussian) distribution, as expected.

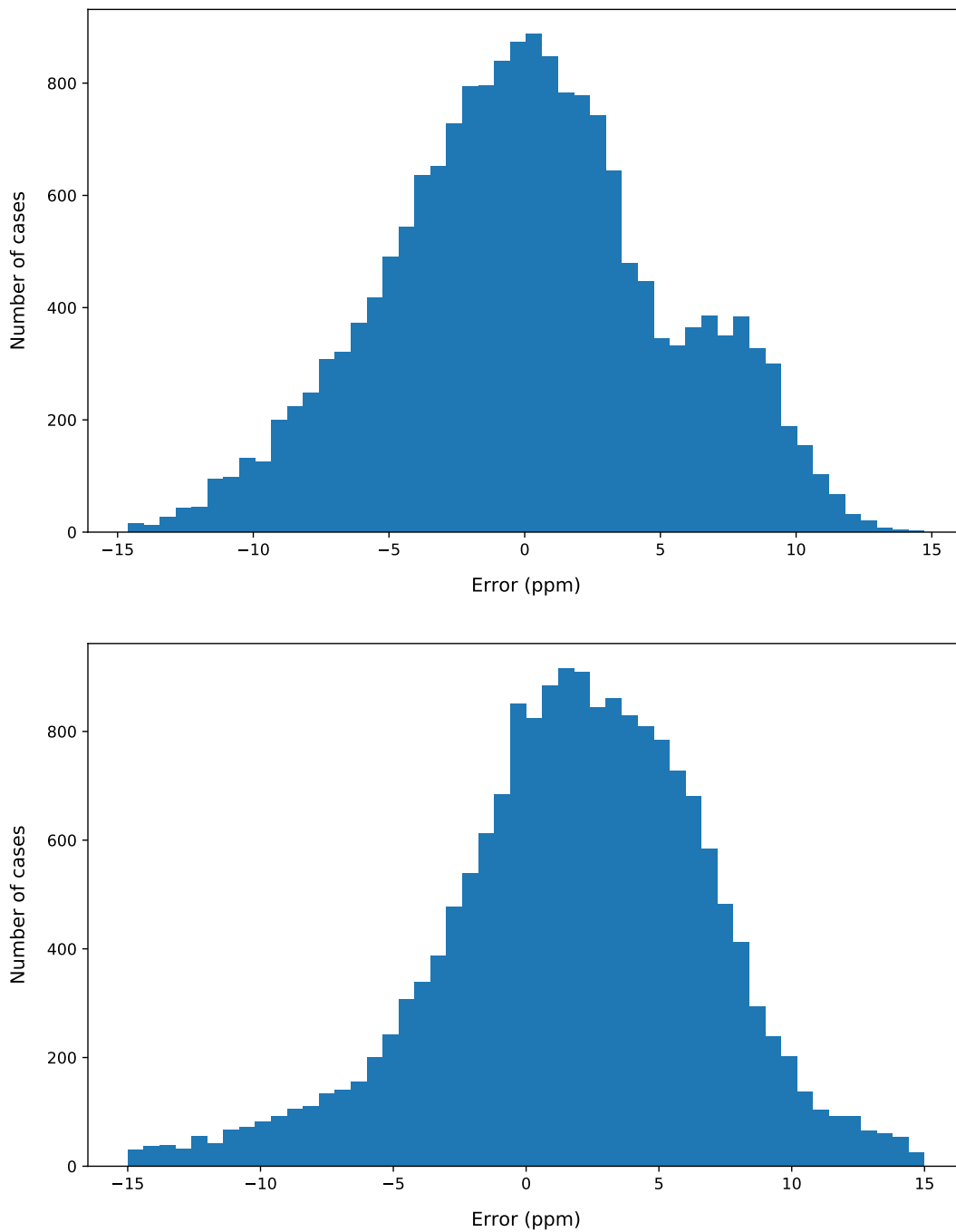


Figure 3.1 Histograms showing wavelength error for both the red (top) and blue (bottom) lasers. Cases where the error was larger than 15 ppm have been cut off to make the distributions easier to see.

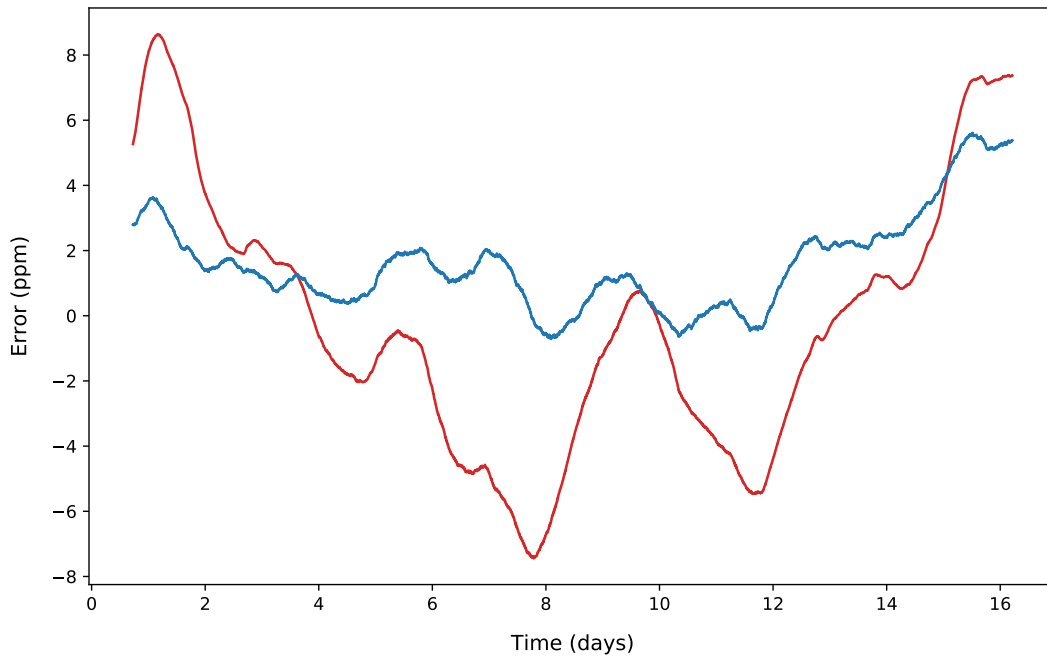


Figure 3.2 Error plotted against time for ELIAS measurements of both the red and blue lasers. This plot was produced using a rolling mean of 1000 points (slightly less than a day’s worth of data) to reduce noise and emphasize trends.

Furthermore, both the accuracy and precision improve when the data is broken into smaller timescales. Broken into 24-hour segments (analogous to recalibrating the device every day), the mean accuracy (both lasers considered) drops to a mere 0.04 ppm with a standard deviation of 3.97 ppm. This is a very impressive result for a device that costs approximately \$100.

3.1.2 Measures of stability

Though the overall precision was similar for the two lasers measured, a closer look at the errors shows some key differences. Figure 3.2 shows that the red laser calibration drifted significantly (± 8 ppm) over the 400 hr test while the blue laser calibration stayed relatively stable (± 3 ppm). Meanwhile, Fig. 3.3 shows that the accuracy of the blue laser calibration varies greatly depending on the wavelength (± 4 ppm) while the red laser is more consistent (± 2 ppm). In other words,

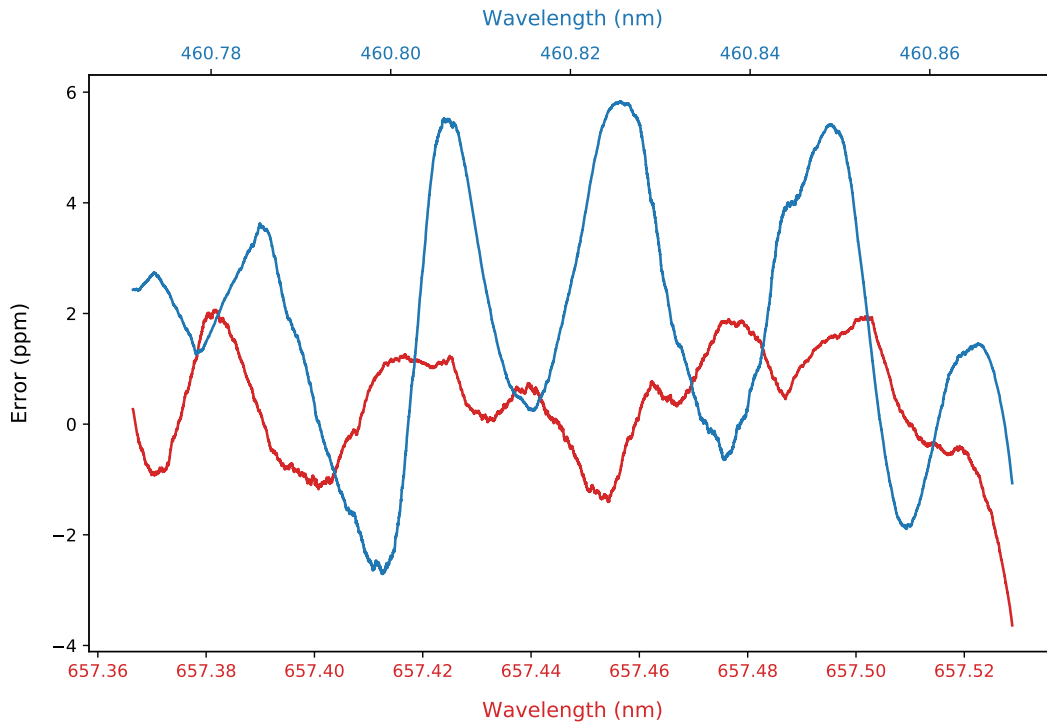


Figure 3.3 Error as a function of wavelength for ELIAS measurements of both the red and blue lasers. The rolling mean method described in Fig. 3.2 was also used in this plot.

measurements made with the ELIAS device were stable in time for the red laser, but stable in wavelength for the blue laser.

Another way to illustrate the difference in temporal stability is by breaking the data into 24-hour segments. This is analogous to recalibrating the device every day. Analyzed thus, the standard deviation error of the red data drops to an average of 2.89 ppm (a 43.5% decrease) while that of the blue data only goes down to 4.99 ppm (an 8.3% decrease).

3.1.3 Allan deviation

An Allan deviation is a way to measure the time scales on which noise occurs in a set of data. The value of a given point is compared to that of a point measured some time τ later. This is particularly useful in differentiating between noise and drift—a large Allan deviation for small values of τ

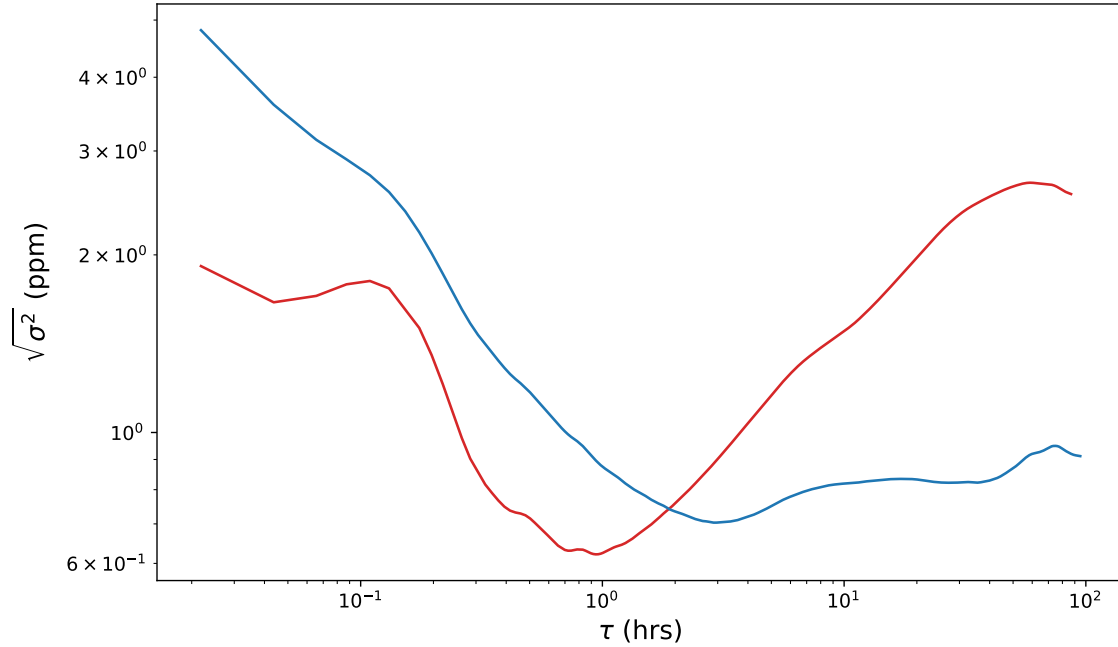


Figure 3.4 Allan deviation error for the red and blue laser measurements.

indicates noise, while a large Allan deviation for large values of τ indicates drift.

The simplest form of Allan deviation, for a given time step τ , is essentially the root-mean-square of differences between the error of points at time t to those at time $t + \tau$. I used a more robust form called the overlapping Allan deviation (included in the Python package "AllanTools"), which is defined as

$$\sigma^2(m\tau_0) = \frac{1}{2(m\tau_0)^2(N-2m)} \sum_{n=1}^{N-2m} (x_{n+2m} - 2x_{n+m} + x_n)^2, \quad (3.1)$$

where m is an integer, τ_0 is the average time between takes, N is the number of takes, and x is the sequence of error measurements. The overlapping Allan deviation is designed for discrete data sets and, therefore, replaces the arbitrary time step τ with discrete multiples of the time τ_0 between each data point.

The Allan deviation in Fig. 3.4 shows that measurements made on the red laser were more consistent over shorter time scales ($\tau < 2$ hrs), while those made on the blue laser were more

consistent over longer time scales ($\tau > 2$ hrs). This matches the information in Figs. 3.2 and 3.3.

3.2 Discussion

3.2.1 High precision, low cost

In Table 1.1, I compared several commercially available wavelength meters. In Table 3.2, I have included the ELIAS wavelength meter. Taking the price into consideration, the ELIAS method's precision is quite impressive. At least when measuring a single TDL, it vastly outperforms devices that cost nearly 80 times as much. The Michelson interferometer is about 30 times more precise, but costs 340 times as much.

Table 3.2 Comparison of ELIAS with other wavelength meters. The commercial devices' precisions have been converted to wavelength-parts per million at 550 nm. The cost of the ELIAS device has been calculated based on the summed cost of its components, excluding the temperature controller.

Wavemeter type	Precision, ppm	Dimensions, cm	Weight, kg	Price
Grating spectrometer [1]	1818	5 x 11 x 15	0.57	\$6563
Integrating sphere [2]	364	9 x 22 x 31	2.5	\$5514
Michelson interferometer [3]	0.18	15 x 32 x 48	12	\$28 026
ELIAS (400 hr)	5.29	20 x 15 x 10	0.5	\$82

3.2.2 Sources of error

The most likely source of error in the ELIAS device is insufficient temperature control. The TEC and thermistor (Fig. 2.1a, f) are both mounted behind the camera, and the plastic housing in which the etalons are mounted has poor thermal conductivity. These factors inevitably cause the connection

between the temperature control and the etalons to be damped and delayed. Without fast-responding temperature control, the etalons are more susceptible to fluctuations in room temperature, which causes the actual pixel responses to shift with regard to their calibrations.

In addition to the temperature control issues, the Allan deviation suggests a potential problem with the lasers. The Allan deviation for the red data is almost identical to that of the color-sensor-based wavelength meter measuring the same laser five years previously [9]. Thus, the laser itself may have something to do with the drift.

The discrepancies between the measurements made on the two lasers is difficult to explain. Possibly the downtime process (see Section 2.2.3) did not work as intended and allowed the camera to cool down between takes. This would result in a small thermal transient at the beginning of each take as the temperature controller responds to the sudden heat produced by the camera turning on. Since the red laser was always measured first, its data may have been more affected by these transients. However, thermal transients don't explain why such significant drift occurred over the course of days, nor why the red data was more precise than the blue on short timescales.

The short-scale noise on the blue laser was likely the result of wavelength-dependent calibration error. Because the wavelength was random for each take, the calibration error manifests as noise in time. The fact that the Allan deviation at the shortest timescale is approximately the same as the amplitude of the fluctuations seen in Fig. 3.3 strengthens this explanation.

3.3 Conclusion

Considering that the ELIAS device was built using less than \$100 of equipment, its performance is encouraging. It achieves an accuracy and precision (respectively) of +0.90 ppm and ± 5.29 ppm over a period of 400 hours, improving to +0.04 ppm and ± 3.94 ppm over 24 hours.

In comparison, wavelengths measured with the color sensor (see Section 1.3), had an accuracy of

11.50 ppm and a precision of 8.46 ppm measuring the blue laser over a period of 41.5 hours [10, 11]. The ELIAS method is 1.6 times more precise and 12.8 times more accurate over a period nearly ten times as long.

Though its current configuration has certain limitations, the ELIAS method could be useful in many labs. For example, if an experiment requires simultaneously measuring two lasers' wavelengths, but the lab only has one wavelength meter, a periodically recalibrated ELIAS device could save thousands of dollars.

3.3.1 Directions for further work

Due to the discrepancies between the blue and red lasers' measurements, more research should be done into the time- and wavelength-based stability of each. Specifically, it is important to know whether the discrepancies are caused by the ELIAS device or the lasers themselves. The 400 hr experiment should be repeated with the blue laser measured first instead of the red, spacing the blue and red measurements equally in time, or taking data with only one laser.

Using more than a thousand pixels could further improve accuracy and precision, but would require a faster method of computation. The Python script I wrote calls the error function $C(\lambda')$ from Eq. (2.6) for each pixel, so computational time likely scales linearly with the number of pixels. Code optimization, a compiled programming language, or machine learning might address this problem.

The maximum calibration range of the device might be improved using more/thinner etalons. If the FSR of the etalon system is large enough, the color filtering on the pixels will cause a detectable difference between corresponding parts of the interference pattern. This would allow the device to measure wavelengths over much or all of the visible spectrum without aliasing.

Finally, and in the very long term, the entire system could be upgraded to a more compact, consumer-friendly device. It could be battery-powered. The etalons, detector, and temperature

control could all be put together in one monolithic block. It could have a designated microcontroller instead of the RPi. These improvements would potentially raise the cost a little, but could lead to an affordable mass-produced device.

Appendix A

Free spectral range and thick etalons

In this thesis, I claimed that thick etalons (*i.e.*, those where the thickness is much greater than the wavelength of the light passing through it), are very sensitive to small changes in wavelength and thickness. In more technical terms, the free spectral range (FSR) is inversely proportional to the number of wavelengths that "fit" in the etalon.

When light passes through an etalon at normal incidence, maximum transmission occurs when the optical path added by a single back-and-forth internal reflection is equal in length to an integer number of wavelengths:

$$2nd = m\lambda, \tag{A.1}$$

where n is the refractive index, d is the etalon's thickness, m is the number of wavelengths that fit along the internal-reflection path, and λ is wavelength. The next peak will occur when $m + 1$ wavelengths fit along the internal-reflection path.

Assuming that the refractive index remains constant, the only two ways to fit another wavelength in the etalon are either to decrease the wavelength or increase the thickness:

$$2nd = (m + 1)(\lambda - \Lambda), \tag{A.2}$$

$$2n(d + \delta) = (m + 1)\lambda, \tag{A.3}$$

where Λ is the free spectral range—the change in wavelength needed to go from one peak to the next—and δ is the corresponding change in thickness. Equation (A.3) easily simplifies to

$$\delta = \frac{\lambda}{2n}, \quad (\text{A.4})$$

and the right-hand sides of Eqs. (A.1) and (A.2) can be equated and solved:

$$\Lambda = \frac{\lambda}{m+1}. \quad (\text{A.5})$$

Knowing that $\lim_{m \rightarrow \infty} (m+1) = m$ and recalling that $\frac{1}{m} = \frac{\lambda}{2nd}$, Eq. (A.5) becomes

$$\Lambda = \frac{\lambda^2}{2nd}. \quad (\text{A.6})$$

Equation (A.4) shows that δ is proportional to wavelength—the interference will be significantly affected by changes in thickness on the order of a wavelength. Equation (A.6), on the other hand, shows that Λ is proportional to wavelength squared divided by thickness. As thickness becomes much larger than wavelength, Λ tends toward zero—many fringes exist in a small range of wavelengths. Note that the derivative

$$\frac{\partial \Lambda}{\partial d} = -\frac{\lambda^2}{2nd^2} \quad (\text{A.7})$$

also tends toward zero in this limit, which explains how the "imperfect flatness" described in Section 2.1.2 is able to affect the interference without much effect on the FSR. The variations in thickness cause large changes to the *position* of the fringes (in wavelength space), but small changes to their *spacing*.

Appendix B

Python code documentation

I developed a Python package to control and analyze the experiment. Due to length, I have not any of the actual code here—the fully annotated package can be found online [14]. In this appendix, I explain some of the more important functions of the package and give instructions for its use.

Running the experiment

The code used to run the experiment is found in the `Device` and `Wavemeter` directories. The file `Wavemeter/pi_interface.py` must be running on a separate computer connected to the Bristol 521 and the internet *before* beginning a data run. The RPi cannot interface directly with the Bristol and requires a non-Linux computer to do so. This second computer receives commands and sends data using *.txt files, located on both computers and accessed via SSH.

The data collection is performed by running `Device/get_data.py`. This script provides a command-line user interface (UI). When beginning a full data run, `get_data` runs a diagnostic test to make sure that the lasers, shutters, camera, and secondary computer are working and communicating properly. If this fails, the user is given the cause(s) of failure.

After a successful diagnostic test, the user is prompted to input a title for the data. Once this is

entered, the RPi will either make a directory with the input title or, if the directory already exists, empty it of all content. *Reusing the title of a data run will delete the existing data.*

The UI then prompts the user to enter the length of time desired for this data run in hours. If zero is entered, the UI will then ask for a time in minutes. Otherwise, it will begin taking data. A progress bar shows how far along the experiment is. Once finished, the script prints the time of completion followed by the title of that run.

Webcam Control

The `get_data.py` script mostly uses classes and functions from `Device/cobbler_code.py` which defines the `Elias` class. This class contains objects representing the webcam and lasers. It also contains several important methods.

`Elias.snap()` takes a series of pictures with the webcam (the default number is 5) and returns the measurement values for only the selected pixels.

`Elias.take(laser)` opens the specified laser shutter, tells the Bristol to start taking a measurement, performs a `snap()`, sums the pictures taken for each pixel, and returns the array of sums. It does not close the shutter since it doesn't know whether the Bristol has finished its measurement.

`Elias.get_wav()` is called immediately after a `take()`. The method checks whether the Bristol has finished its measurement. Once it has, it closes the shutter and returns the wavelength measurement.

`Elias.hold(t)` keeps the camera warm for a specified number of seconds `t` by constantly taking pictures and throwing away the data. This function is called between takes.

Laser and shutter control

The lasers and shutters are controlled from `Device/control_lasers.py`. Because each laser requires a unique interface, the script defines a unique class for each one. Originally, a 408 nm laser

was also included in the experiment, and the control class for that laser is still in the script. All laser classes contain the same methods, which allows `get_data.py` to handle them all the same. Internally, however, each class performs unique functions to interface with its respective laser.

The `Red` class requires that the RPi be connected to a New Focus "Vortex 6000" laser controller through an RS-232 serial cable. A USB-serial adapter is required for the RPi. The `Blue` class is designed to control a New Focus "TLB-6700" laser controller. Because no driver exists for the RPi, the control is sent to the laser's analog frequency control input. The RPi generates a PWM signal using its GPIO terminals. That signal must then be rectified and converted to an analog voltage from -3 to 3 V using low-pass filtering and a voltage divider. The `Ultraviolet` class interfaces with a Toptica "DLCPro" laser which, in the end, was not used in this experiment.

Each laser control class has a `shutter` attribute: a GPIO object that can be either on or off. The state of this object triggers the state of the shutter. The shutters are externally powered solenoids (see Appendix C).

Data analysis

The code used to analyze the data is found in the `Analysis` directory. The `DataSet` object, defined in `Analysis/wave_meter_source.py`, contains methods for calibration, wavelength calculation, error analysis, and plotting. The file `Analysis/analyze_data.py` performs the full analysis (described in Section 3.1) by creating a `DataSet` object. The data given to the object is determined using the parameters assigned in the first few lines of `analyze_data`. The plots in this thesis were made using `DataSet` class methods as well as a few simple functions defined in `Analysis/compare_lasers.py`.

Appendix C

Shutter system design

I designed and built an automated shutter system (Fig. 2.3c) so that the experiment could measure two lasers individually (see Section 2.2.1). The shutters themselves are solenoid motors mounted such that the arm blocks the beam path when extended. When the solenoid receives power, the arm is retracted out of the beam path, allowing the beam to pass.

The control mechanism is shown in Fig. C.1. One of the RPi's GPIO pins connects to the base of a Darlington transistor. When the pin is turned on, the transistor allows current to flow from the power supply to the solenoid. To prevent overheating, heat sinks were attached to both the transistors and the solenoids.

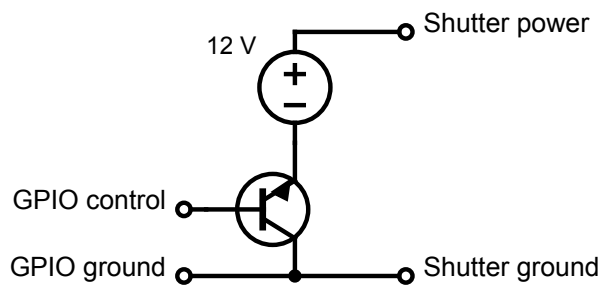


Figure C.1 Circuit used to control the shutters.

Appendix D

Blue laser controller

Due to incompatibility issues between the RPi and the blue laser controller, that laser's wavelength must be adjusted via an analog input. The controller receives an input voltage between -3 and 3 V and translates it to a wavelength-tuning value between the minimum and maximum wavelengths of the laser head.

The RPi cannot provide precise voltages from its GPIO terminals; they can only be set to 0 V or 3.3 V. However, it can provide a precise *average* voltage using a pulse-width modulation (PWM) signal. A PWM signal oscillates at a high frequency between two values (in this case, 0 and 3.3 V) and adjusts the time spent at each value. The percentage of time spent at the higher value is known as the duty cycle.

The circuit shown in Fig. D.1 converts the PWM signal from the RPi to an analog voltage from -3 to 3 V. The supply voltages for the op-amps are 12 V and -9 V. The resulting voltage provided to the laser controller is approximately

$$V = -3 + 6D, \tag{D.1}$$

where D is the duty cycle, which ranges from zero to one.

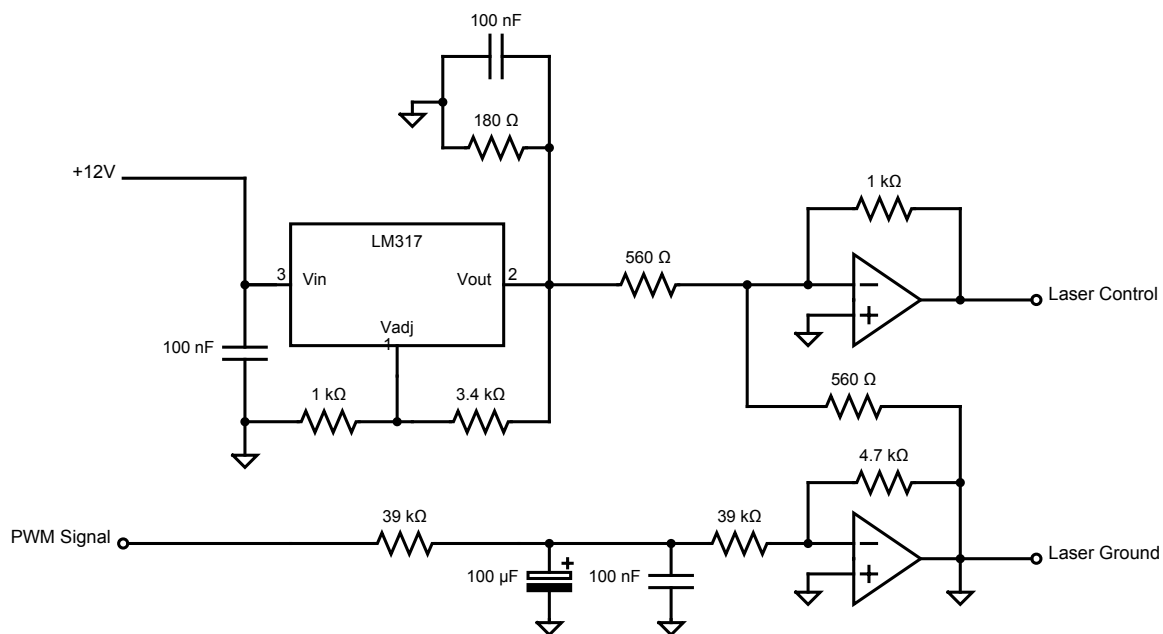


Figure D.1 Circuit used to control the blue laser.

Bibliography

- [1] “HR4000CG-UV-NIR Spectrometer | High Resolution | Ocean Insight,” <https://www.oceaninsight.com/products/spectrometers/high-resolution/hr4000cg-uv-nir/>.
- [2] “OMH-6790B,” <https://www.newport.com/p/OMH-6790B>.
- [3] “Thorlabs - OSA201C Fourier Transform Optical Spectrum Analyzer,” <https://www.thorlabs.com/thorproduct.cfm?partnumber=OSA201C>.
- [4] R. F. Nabiev, C. J. Chang-Hasnain, L. E. Eng, and K.-Y. Lau, “Monolithic wavelength meter and photodetector using a wavelength dependent reflector,” 1996, U.S. Patent 5760419A.
- [5] M. Mazilu, T. Vettenburg, A. D. Falco, and K. Dholakia, “Random super-prism wavelength meter,” *Optics Letters* **39**, 96–99 (2014).
- [6] D. F. Gray, K. A. Smith, , and F. B. Dunning, “Simple compact Fizeau wavemeter,” *Applied Optics* **25**, 1339–1343 (1986).
- [7] N. Konishi, T. Suzuki, Y. Taira, H. Kato, and T. Kasuya, “High precision wavelength meter with Fabry-Perot optics,” *Applied Physics* **25**, 311–316 (1981).
- [8] “Scanning Fabry-Perot Interferometers,” https://www.thorlabs.com/newgrouppage9.cfm?objectgroup_id=859.

- [9] T. B. Jones, N. Otterstrom, J. Jackson, J. Archibald, and D. S. Durfee, “Laser wavelength metrology with color sensor chips,” *Optics Express* **23**, 32471–32480 (2015).
- [10] T. Jones, Bachelor’s thesis, Brigham Young University, 2015.
- [11] N. Otterstrom, Bachelor’s thesis, Brigham Young University, 2015.
- [12] G. Langer, A. Hochreiner, P. Burgholzer, and T. Berer, “A webcam in Bayer-mode as a light beam profiler for the near infra-red,” *Optics Communications* **262**, 97–102 (2006).
- [13] F. Cignoli, S. D. Iuliiis, and G. Zizak, “A Webcam as a Light Probe Beam Profiler,” *Applied Spectroscopy* **58**, 1372–1375 (2004).
- [14] J. N. Porter, “ELIAS software,” <https://doi.org/10.5281/zenodo.4008685>, 2020.
- [15] J. N. Porter, J. S. Jackson, D. S. Durfee, and R. L. Sandberg, “Laser wavelength metrology with low-finesse etalons and Bayer filters,” *Optics Express* **28**, 37788–37797 (2020).
- [16] “Camera Module - Raspberry Pi Documentation,” <https://www.raspberrypi.org/documentation/hardware/camera/>.
- [17] “IMX219 - Electronics Datasheet,” <https://www.electronicdatasheets.com/download/5721ed8ce34e24fd697a913a.pdf?format=pdf>.
- [18] “ILX Lightwave LDT-5412 User Manual,” <https://www.manualslib.com/manual/769138/Ilx-Lightwave-Ldt-5412.html>, discontinued model.

Index

- color sensor, 4
- cost function, 17
- ELIAS, 5
 - benefits and drawbacks, 5
 - design, 7–11
- etalon, 2
 - Fabry-Perot, 4, 9
 - in ELIAS device, 9–10
- etaloning, 2–4
 - free spectral range, 3, 29
 - thick-film, 3, 29
 - with multiple etalons, 11
- lasers used in experiment, 12
- ppm (parts per million), 19
- Raspberry Pi, 9, 12, 14
 - Picamera, 9
- take, 15
- temperature control, 11, 25
- wavelength meter
 - alternative designs, 2, 4, 5
 - commercially available, 1
- webcam
 - advantages of, 4